

An experimental investigation on slope stability under drawdown conditions using transparent soils

Wanghua Sui¹ · Guosheng Zheng¹

Received: 15 January 2017 / Accepted: 23 May 2017 / Published online: 27 June 2017
© Springer-Verlag Berlin Heidelberg 2017

Abstract This paper presents an experimental investigation into slope failure during water-level drawdown using transparent soil. The internal characteristics of slope failure are not well-known due to the limitations of the techniques used in the experiments conducted to date. In this study, transparent soil is used to visualize the process of slope failure. We developed a water-level control system to implement simulation of the drawdown of the water level at various speeds and used a charge-coupled device camera to capture images during the entire slope failure process. Particle image velocimetry was used to measure the displacement of the sand particles and identify the sliding zones. The flow paths of the fluid inside the slope were illuminated using an organic dye. The results show that the slope failure process can be divided into two stages: surface and overall sliding. The overall sliding of the slope is caused by the gradual development of partial instability, and the failure mode is a cyclic failure. The slope angle is different above and below the water level during the process of sliding. In our experiments, the slope angle is about 20° above the water level, which is the same as the final stable slope angle, and about 35° below the water level, which is the same as the initial slope angle. This means that the drawdown influences the angle above the water level but has little influence on the angle below the water level. The results of this

paper provide a better understanding of the physical behavior and failure mode of soil slopes caused by drawdowns near the coast.

Keywords Slope stability · Water drawdown · Transparent soil

Introduction

The stability of a slope depends on the properties of the soil, geometry of the slope, and the interaction between the internal and external forces that are acting on the surface of the soil (Berilgen 2007). However, changes in the internal and external forces caused by water levels may reduce slope stability due to rapid drawdown, which then leads to slope failure. Slope failures near the coast can be generated by sea-level change and waves. They are a major threat not only to the oil and offshore industries, but also to the marine environment and coastal facilities. Much effort has been made to characterize and understand slope failures that are related to water drawdown conditions. Mayer (1936) first discussed the details of the failures of four earth dams caused by the drawdown of the reservoir. Della Seta et al. (2013) analyzed slope instability in coastal areas caused by sea-level changes. Their results show that landslides occur not only in the process of sea-level rise, but also in the process of sea-level drawdown. The work of Hutton and Syvitski (2004) indicates that more sediment failures occur during periods of falling sea levels than periods where they are rising. Morgenstern (1963) used a method of slices to estimate the safety factor of slopes under rapidly declining water levels and presented a set of charts to analyze the stability of earth slopes during rapid drawdown. The finite-element method and kinematic approach of limit analysis have also been used to analyze slope stability under drawdown conditions (Lane and

✉ Wanghua Sui
suiwanghua@cumt.edu.cn

Guosheng Zheng
guoshengzheng@cumt.edu.cn

¹ School of Resources and Geosciences, State Key Laboratory for Geomechanics and Deep Underground Engineering, China University of Mining and Technology, 1 University Ave (Daxuehu), Xuzhou, Jiangsu 221116, China

Griffiths 2000; Viratjandr and Michalowski 2006). Other researchers have used scale model tests to investigate slope stability failure induced by the drawdown of water levels (Jia et al. 2009; Li et al. 2008; Wang et al. 2012); the slip surface, slope geometry, pore pressure changes, and the type of slope failure were discussed in these previous publications.

Although the mechanisms of landslides under water have been widely discussed, the characteristics of slope failure, such as the sliding zones and variations of the slope angle, and slope failure properties, such as the speed of the landslide and the flow path, are uncertain due to limitations when carrying out experiments. Ma and Duan (2007) showed that the shape and speed of a landslide under water as well as the slope angle play an important role in generating tsunamis. Therefore, it is critical to have a better understanding of the characteristics and properties of slope failure under drawdown conditions. Sensors and strain gauges can be embedded into the soil to obtain the deformation information in scale model tests. However, sensors and strain gauges can contribute to the deformation of soils and continuous data on soil deformation cannot be always obtained. Therefore, the solution used in this study is a technique utilizing transparent soil in order to overcome these limitations and obtain data on continuous movement and deformations with no other influences.

This paper presents an experimental investigation on the characteristics of landslides and the slope failure process under drawdown conditions using transparent soil. The particle motions, slope angle variations, and the flow paths are examined and discussed.

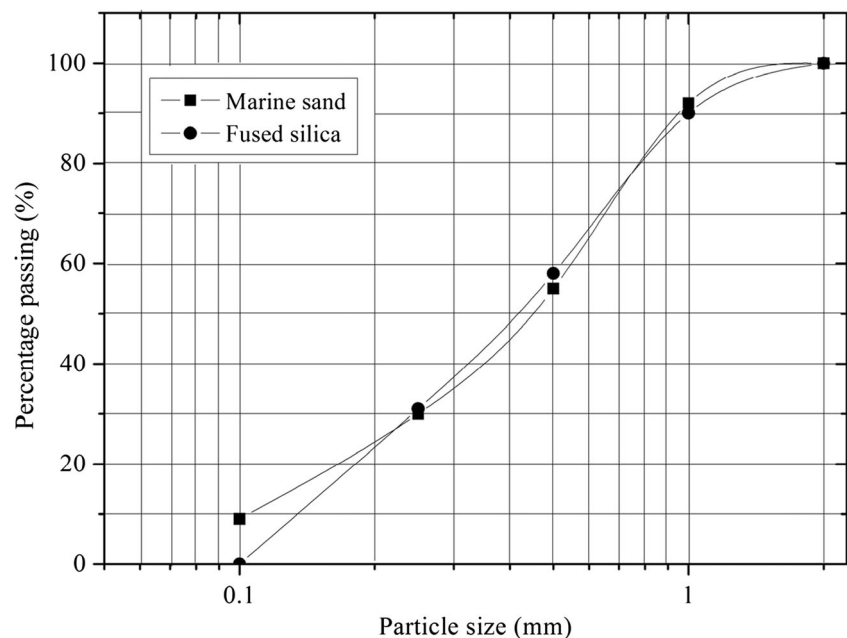
Materials and methods

Materials

Transparent soil is a two-phase medium made by matching the refractive index (RI) of solids (which represent the soil skeleton) and saturating fluids so that there is no difference between the two, or no refraction and reflection, and thus the mixed medium becomes transparent (Iskander et al. 2015). Transparent soil has been used by many researchers in their investigations, and the geotechnical properties of transparent soil were found to be similar to those of natural sands or clays.

The transparent soil used in this study is made of fused silica and mineral oils with the same RI. Fused silica with a grain size that ranges from 0.1 to 2.0 mm is used, which is manufactured by Jiangsu Kaida Silica Co., Ltd. China. Figure 1 shows the particle gradation curve of the marine sand sampled from coast of the Yellow Sea and fused silica used in this experiment. Fused silica has been widely used in transparent modeling (Bathurst and Ezzein 2015; Guzman et al. 2015; Ferreira and Zornberg 2015). Mineral oils A and B were mixed and applied as the pore fluid. Mineral oils A and B have a specific gravity of 0.812 and 0.844, a kinematic viscosity of 5 and $10 \times 10^{-6} \text{ m}^2/\text{s}$, and an RI of 1.4662 and 1.4397, respectively. The mixture was mixed using oil A and B at a ratio of 2:1 by volume. Its RI is equal to that of the fused silica when the temperature reaches 30 °C. The temperature maintains at 30 °C during the test due to the fact that the RI of the oils varies with temperature (Sui et al.

Fig. 1 The particle gradation curve of the marine sand and fused silica



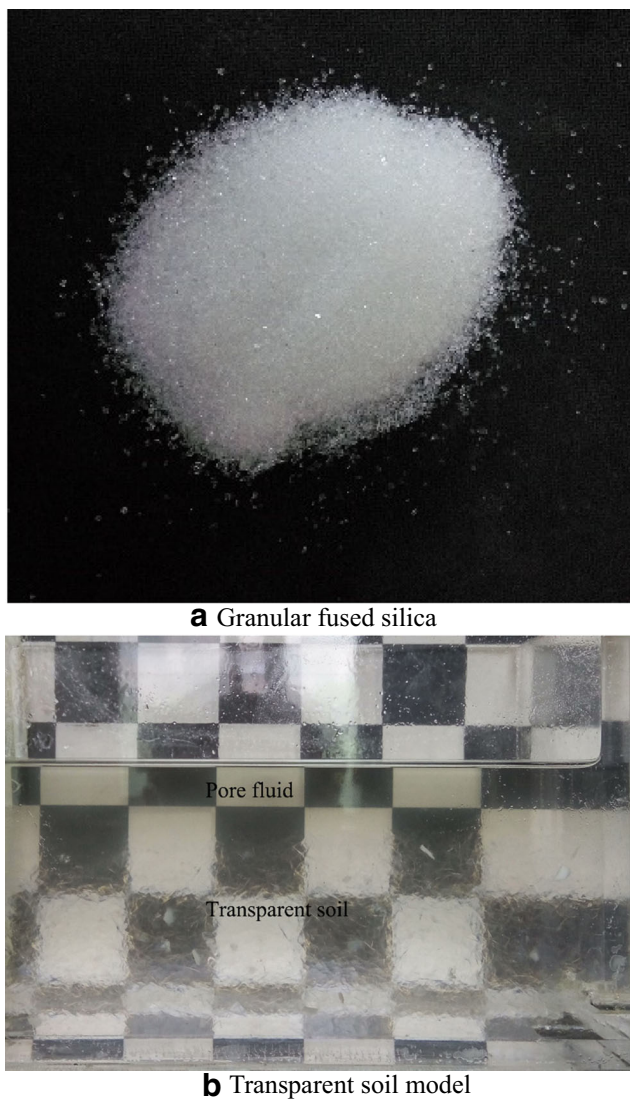


Fig. 2 Materials and model setup: (a) granular fused silica; and (b) transparent soil model

2015). Figure 2a shows the dry fused silica and Fig. 2b shows the transparent soil model. The physical properties of the fused silica used in this study are summarized in Table 1 along with those of Chinese standard sand obtained from China ISO Standard Sand Co. LTD and marine sand obtained from the Yellow Sea. It should be noted

that the fused silica can be used to simulate marine sand in this experiment.

Experimental setup

Figure 3 shows the experimental setup, which is placed onto a precision optical table. The setup consists of a transparent model, a water-level control system, an image acquisition system, and an image processing system.

A transparent Plexiglas[®] mold with internal dimensions of $41 \times 10 \times 20$ cm was used to accommodate the transparent slope model, and the geometry of the slope model is shown in Fig. 3b. The slope model consisted of a homogeneous soil slope with an up-slope portion that was 17 cm thick and down-slope portion that was 3 cm thick. The slope angle was 35° and the net height of the slope model was 14 cm. The distance extended backward from the crest was 5 cm. The distance extended beyond the toe of the slope was 10 cm.

A water-level control system was developed to simulate the drawdown, which consisted of a Plexiglas[®] model, peristaltic pump, stepper motor, and sliding table. Liquid flowed in from the inlet opening through the peristaltic pump and flowed out through the outlet opening. The outlet opening was fixed onto the sliding table, which was controlled by the stepper motor. Liquid flowed out from the water-level control hole if the water level was higher than the set value. There were two filters in the model; the one on the left was used to ensure the stability of the hydrostatic pressure on the left side of the slope, and the filter on the right was used to stop the sand from being washed away by the liquid.

The image acquisition and analysis system consisted of a charge-coupled device (CCD) camera and a laser light for illuminating purposes. The CCD camera has a resolution of 1024×768 pixels and a maximum frame rate of 30 frames per second (fps). The CCD camera was controlled by a computer.

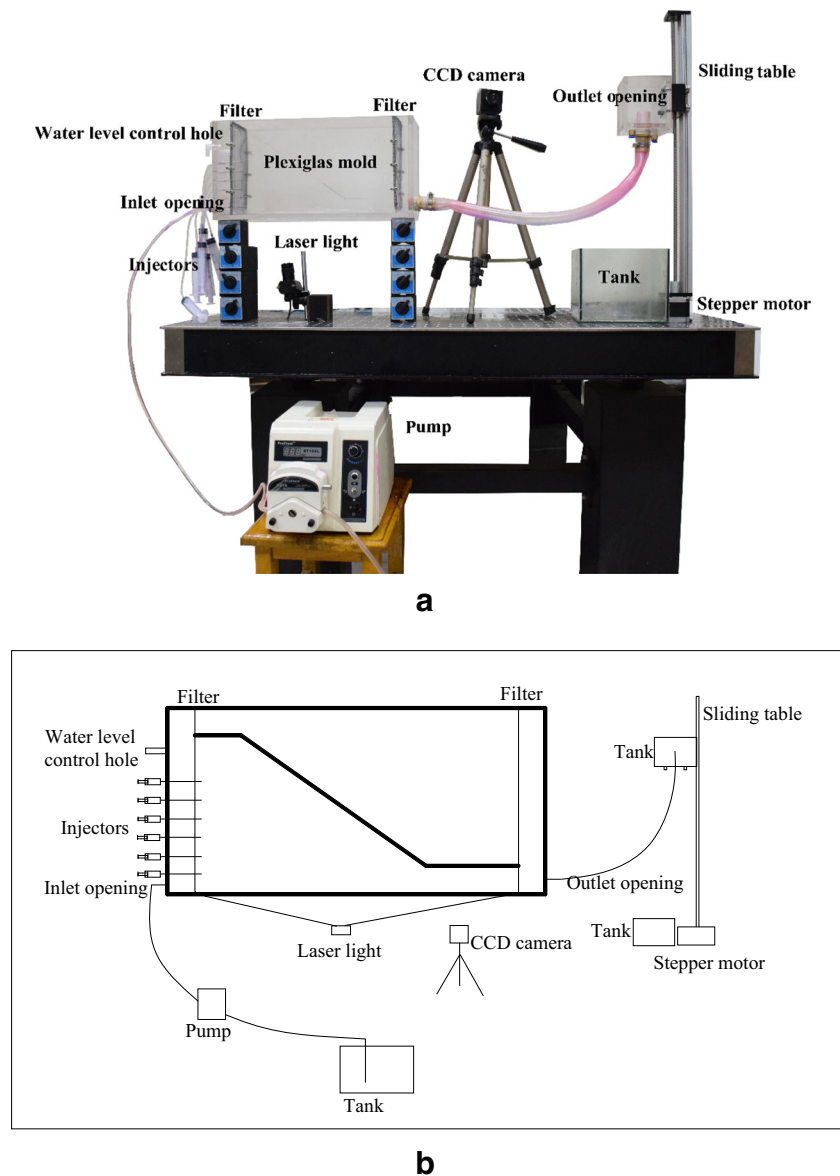
Particle image velocimetry (PIV) was used to measure the velocity of the sand particles and identify the sliding zones. PIV is also known as digital image correlation (DIC) or cross-correlation. It is a classic pattern-recognition technique where two images are compared to obtain the relative displacement

Table 1 Physical properties of fused silica, Chinese standard sand, and marine sand

	G_s	ρ_{\max} (g/cm^3)	ρ_{\min} (g/cm^3)	e_{\max}	e_{\min}	K (cm/s)	φ ($^\circ$)
Fused silica	2.2	1.46	1.22	0.8	0.51	0.0074	42
Standard sand	2.65	1.75	1.50	0.76	0.51	0.0067	40
Marine sand	2.69	1.74	1.51	0.76	0.54	0.0072	43

Note: G_s is specific gravity, ρ_{\max} the maximum and ρ_{\min} the minimum dry density, e_{\max} the maximum and e_{\min} the minimum void ratio, K Hydraulic conductivity and φ angle of internal friction.

Fig. 3 (a) Photo and (b) schematic of the experimental setup. CCD charge-coupled device



between these particles (Liu and Iskander 2010). In geotechnical engineering applications, DIC has been used to measure and analyze soil deformation (Iskander et al. 2015; Mehdi et al. 2015; Ahmed and Iskander 2011; Liu 2009).

Test procedures

The model box was first partially filled with the mineral oils. The total volume of the slope model was 3150 cm^3 and the relative density of the fused silica was set to 50%. A total of 4.2 kg of soil was used to construct the slope model. The fused silica was divided into five parts and gradually immersed into the mineral oils. A vacuum pump was used to de-aerate the mixture for about 1 h until the fused silica was saturated and turned transparent. This procedure was repeated until all of the

fused silica were immersed into the mineral oils to create the transparent soil slope.

After preparing the sample, the laser light source was adjusted to illuminate the section of interest. The CCD camera was then connected at an acquisition rate of 3.75 fps. Background images were taken before the water level started to decline. Next, the peristaltic pump was turned on and the water-level drawdown was adjusted to a rate of 8 cm/min. Once the peristaltic pump and the stepper motor were activated, a series of images were taken during the drawdown process. The tests were stopped when the particles on the slope stopped sliding. Then the rate of the drawdown was varied to 4, 2, 1, and 0.5 cm/min for the four tests that followed. Finally, an oily fluorescent dye was injected into the transparent soil model to identify the flow paths inside the slope.

Results

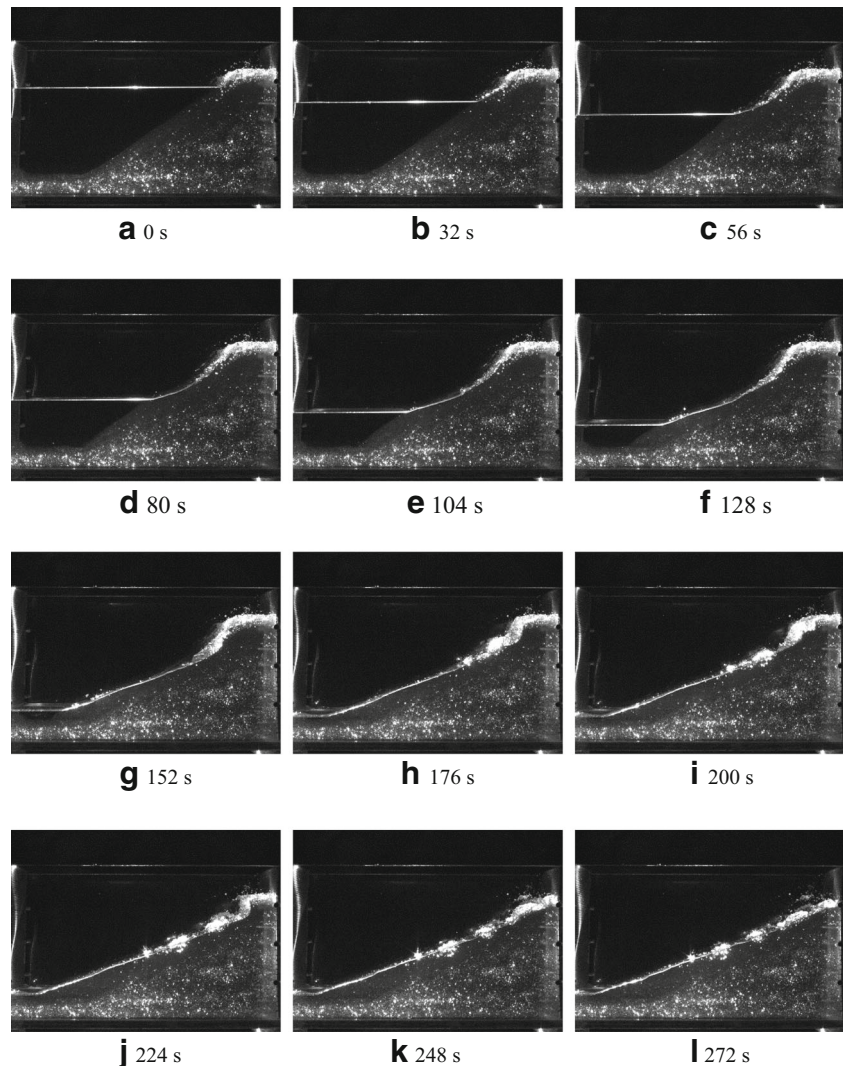
About 1020 images for each test were obtained during the entire modeling of the slope failure process. This process can be examined in two stages: surface sliding and overall sliding. Figure 4 shows 12 of the selected images with a time interval of about 24 s to visualize the slope failure process for a drawdown rate of 4 cm/min. Figure 5 shows the contour maps of the sliding field at different times that correspond to the process shown in Fig. 4. The dotted curves represent the initial water level and the solid lines represent the continually decreasing water levels. During sliding, the sand particles began to slide at the top of the liquid surface when the water level dropped to 12.40 cm. The sand particles on the slope gradually rolled to the toe of the slope. The maximum sliding velocity was 1.80 cm/s during this stage, which occurred at the surface of the slope and changed the slope angle, but the slope was not damaged. In the overall failure stage, which started

from the 104th second, the sand particles began to slide due to seepage erosion on the face of the slope (Figs. 4e and 5e). The maximum sliding velocity was 1.65 cm/s during this stage. This stage changed the shape of the slope.

Figure 5b shows that the particles began to slide at the point where the liquid level was reduced, i.e., when the water level declined to a certain point. With continual decline of the water level, the speed of the particle sliding and the area of the sliding zone both gradually increased. It was found that the sliding speed on the surface is greater than that inside the slope, and the sliding speed at the center of the sliding body is higher than that at the edges. The sliding zone area in the second stage (overall sliding) is larger than that in the first stage (surface sliding). Figure 5 also shows that the overall sliding of the slope is caused by the gradual development of partial instability, and the failure mode is a cyclic failure.

Figure 6 shows the relationships among sliding speed, water level drawdown, and time, while Fig. 6a shows the

Fig. 4 Images captured by charge-coupled device (CCD) camera at different times: (a) 0 s; (b) 32 s; (c) 56 s; (d) 80 s; (e) 104 s; (f) 128 s; (g) 152 s; (h) 176 s; (I) 200 s; (j) 224 s; (k) 248 s; and (l) 272 s



relationship between sliding speed and time. It is obvious that the horizontal speed of the sand particles is greater than their vertical speed. Figure 6b shows the relationship between the rate of drawdown and sliding speed. It was found that a higher rate of drawdown results in a landslide that moves with greater speed. This is because a higher rate of drawdown caused a greater hydraulic gradient and a greater seepage force from upstream to downstream. When the rate of drawdown is 0.5 cm/min, the sliding speed of the particles is greater than that for a rate of 1 cm/min when the water level decreased to 9 cm. This is because the second stage (overall sliding) started when the rate of drainage is 0.5 cm/min.

Figures 4 and 5 also show that there are two different slope angles due to the water level during particle sliding. The slope angle is about 20° above the water level, which is the same as the final stable slope angle. Below the water level, the slope angle is about 35° , which is the same as the initial slope angle.

Fig. 5 Contour maps of the sliding field at different times: (a) 0 s; (b) 32 s; (c) 56 s; (d) 80 s; (e) 104 s; (f) 128 s; (g) 152 s; (h) 176 s; (i) 200 s; (j) 224 s; (k) 248 s; and (l) 272 s

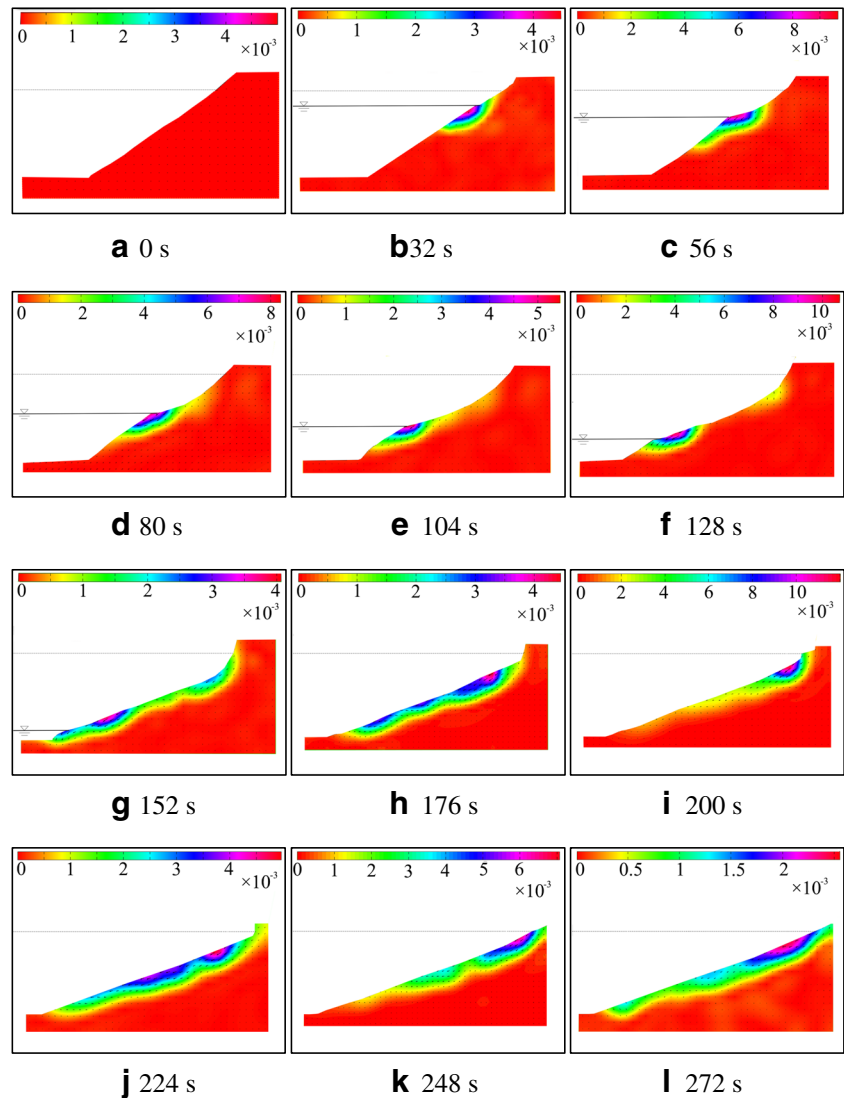


Figure 7 shows the final geometry of the slope when the rate of drawdown is 4 cm/min. The final geometries of the slope for the different rates of drawdown were then drawn into one schematic, and it was observed that the rate of drawdown has little influence on the final geometry of the slope.

Organic dye was injected into the slope during the slope failure process to obtain the flow paths. Figure 7 also shows the flow paths inside the slope 50 min after injection. It should be noted that the liquid is flowing horizontally and exits the slope surface, thus creating seepage on the slope.

Discussion

The image analysis showed that slope seepage occurs when the water level declines to a certain point. Figure 8 is a schematic diagram of the stress found when there is slope seepage,

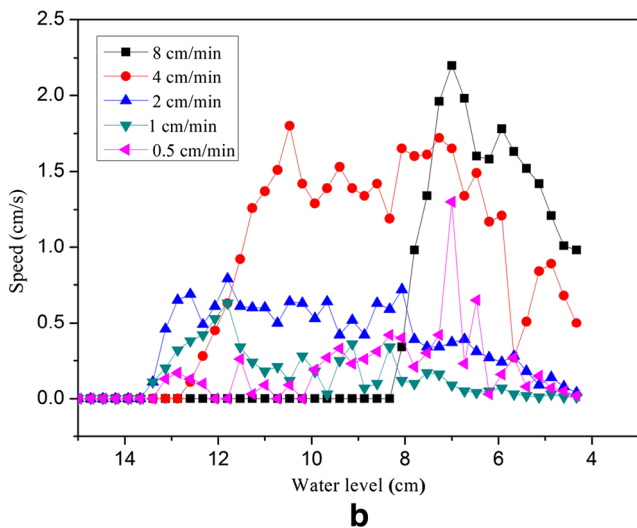
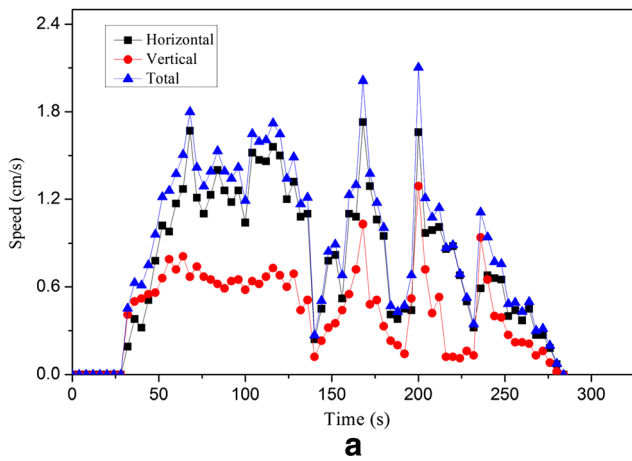


Fig. 6 Relationship between the maximum speed and (a) time and (b) water level

and the expression of the factor of safety in this condition is as follows:

$$F = \frac{\gamma' \tan \varphi}{\gamma_{sat} \tan \beta} \quad (1)$$

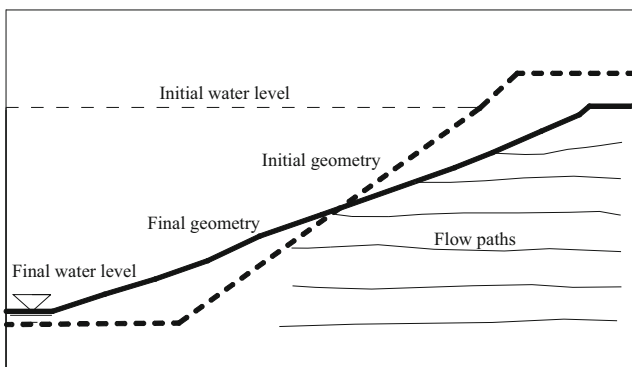


Fig. 7 Final geometry of the slope and flow paths inside the slope

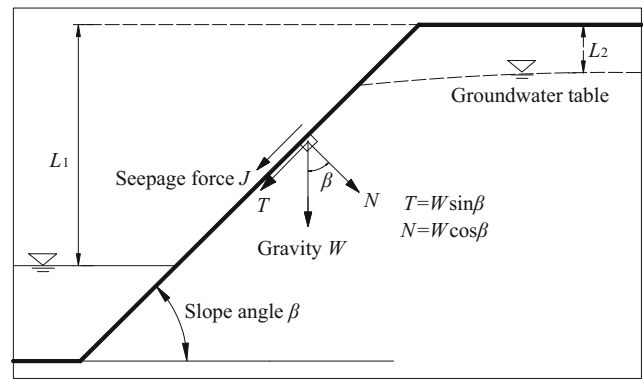


Fig. 8 Schematic diagram of stress inside slope

Substituting the known parameters into Eq. 1 yields a final slope angle of 20° when the factor of safety is 1. The final slope angles obtained from the tests are summarized in Table 2. It is obvious that the values obtained from the tests are in good agreement with those calculated using Eq. 1.

Viratjandr and Michalowski (2006) analyzed slope stability during water level drawdown when cohesion is 0, and provided an expression of the factor of safety as follows:

$$F = \tan \varphi \frac{\frac{\gamma_w}{\gamma} \left(1 - \frac{L_1}{H}\right)^2 \sin^2 \beta - \frac{\gamma_w}{\gamma} \left(1 - \frac{L_2}{H}\right)^2 + \cos^2 \beta}{\left[1 - \frac{\gamma_w}{\gamma} \left(1 - \frac{L_1}{H}\right)^2\right] \sin \beta \cos \beta} \quad (2)$$

The factor of safety was calculated before the sand particles began to slide; according to the results, the sand particles began to slide when the water level declined to different points for different rates of drawdown. Next, the factor of safety was calculated when the particles began to slide. Figure 9 shows the relationships among the factor of safety, sliding speed, and water level. It should be noted that the sand particles begin to slide when the factor of safety is about 1 at the rate of drawdown of 2, 1, and 0.5 cm/min. However, the factor of safety is less than 1 when the rate of drawdown is 4 and 8 cm/min. This indicates that the theoretically calculated results are less than the actual values when the drawdown is faster.

This work aims to investigate the features of the slope failure during drawdown conditions, and large-scale model tests will be more costly. Therefore, this study did not match a specific slope prototype. However, according to general principles of soil mechanics, the stability of a slope composed

Table 2 Final slope angles under different drawdown conditions

Rate of drawdown (cm/min)	8	4	2	1	0.5
Final slope angle ($^\circ$)	21	20	21	19	20

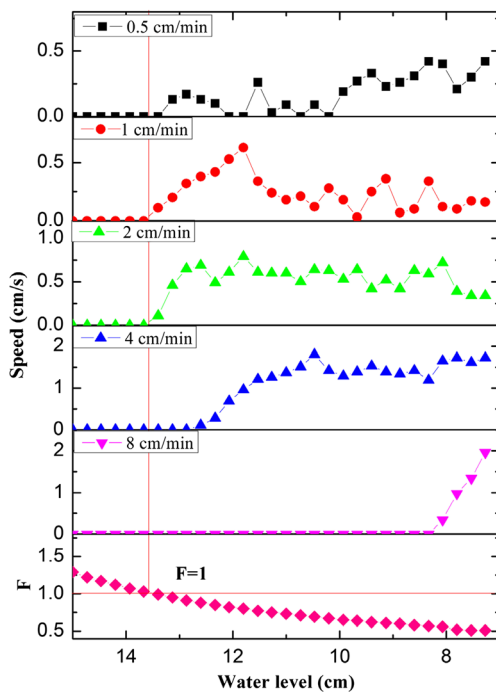


Fig. 9 Relationships among factor of safety, sliding speed, and water level

of granular materials is mainly determined by the slope angle and angle of internal friction of the material rather than the height of the slope. The similarity of the angle of internal friction of the sand used in the experiment and that of natural sand ensures the reliability of the scale model test. The decision on the model size was based on a very simplified engineering geological conditions. Obviously, the experimental conditions should be modified to be more representative of geological conditions in future work. Other properties of sand, such as permeability, density, and particle size distribution also have significant influence on the stability of slopes; therefore, further investigation is needed.

Conclusions

Particle sliding, slope angle changes, and the flow paths in the process of slope failure under drawdown conditions are observed in this study using transparent soil. The following conclusions are made:

- (1) The process of slope failure during water-level drawdown can be examined in two stages: surface sliding and overall sliding. The horizontal speed of the sand particles is greater than their vertical speed during failure. The overall sliding is caused by the gradual development of particle instability.

- (2) The rate of drawdown influences the sliding speed but has little influence on the final geometry of the slope. The factor of safety calculated using a theoretical equation is less than the actual value when the rate of drawdown is fast.
- (3) The slope angle is different above and below the water level during the sliding process. The final slope angle obtained from the tests is in good agreement with those calculated using an equation that takes into consideration the seepage force.
- (4) In the slope failure process, the liquid flows horizontally. Finally, the liquid exits the slope surface, creating seepage on the slope.

This paper provides an improved understanding on slope failure under drawdown conditions. The results can be used to design the rate of drawdown and slope anti-seepage and predict the final geometry of slopes in coastal engineering. In addition, this paper provides a new method to research coastal landslides.

Acknowledgments The authors would like to acknowledge the financial support of the Natural Science Foundation of China under Grant No. 41472268, 111 Project under Grant No. B14021, and a Project Funded by the Priority Academic Program Development of Jiangsu Higher Education Institutions. Assistance from Dr. Yue Gao in the testing is greatly appreciated.

References

- Ahmed M, Iskander M (2011) Transparent soil model tests and FE analyses on tunneling induced ground settlement. *Geo-Frontiers Congress 2011: Advances in Geotechnical Engineering*, ASCE, Virginia, pp:3381–3390. doi:10.1061/41165(397)346
- Bathurst RJ, Ezzein FM (2015) Geogrid and soil displacement observations during pullout using a transparent granular soil. *Geotech Test J* 5:673–685. doi:10.1520/GTJ20140145
- Berilgen MM (2007) Investigation of stability of slopes under drawdown conditions. *Comput Geotech* 34:81–91. doi:10.1016/j.compgeo.2006.10.004
- Della Seta M, Martino S, Mugnozza G (2013) Quaternary sea-level change and slope instability in coastal areas: insights from the Vasto landslide (Adriatic coast, central Italy). *Geomorphology* 201:462–478. doi:10.1016/j.geomorph.2013.07.019
- Ferreira J, Zornberg J (2015) A transparent pullout testing device for 3D evaluation of soil–geogrid interaction. *Geotech Test J* 5:686–707. doi:10.1520/GTJ20140198
- Guzmana I, Iskander M, Blessca S (2015) Observations of projectile penetration into a transparent soil. *Mech Res Commun* 70:4–11. doi:10.1016/j.mechrescom.2015.08.008
- Hutton E, Syvitski J (2004) Advances in the numerical modeling of sediment failure during the development of a continental margin. *Mar Geol* 3:367–380. doi:10.1016/S0025-3227(03)00316-5
- Iskander M, Bathurst R, Omidvar M (2015) Past, present, and future of transparent soils. *Geotech Test J* 5:557–573. doi:10.1520/GTJ20150079

- Jia G, Zhan T, Chen Y, Fredlund D (2009) Performance of a large-scale slope model subjected to rising and lowering water levels. *Eng Geol* 106:92–103. doi:[10.1016/j.enggeo.2009.03.003](https://doi.org/10.1016/j.enggeo.2009.03.003)
- Lane P, Griffiths D (2000) Assessment of stability of slopes under draw-down conditions. *J Geotech Geoenviron Eng* 5:443–450. doi:[10.1061/\(ASCE\)1090-0241\(2000\)126:5\(443\)](https://doi.org/10.1061/(ASCE)1090-0241(2000)126:5(443))
- Li S, Knappett J, Feng X (2008) Centrifugal test on slope instability induced by rise and fall of reservoir water level. *Chinese J Rock Mech Eng* 8:1586–1593 [in Chinese]
- Liu J (2009) Visualizing 3-D internal soil deformation using laser speckle and transparent soil techniques. Characterization, modeling, and performance of geomaterials: selected papers from the 2009 Geo Hunan International Conference, ASCE, Virginia, pp. 123–8
- Liu J, Iskander M (2010) Modelling capacity of transparent soil. *Can Geotech J* 47:451–460. doi:[10.1139/T09-116](https://doi.org/10.1139/T09-116)
- Ma W, Duan W (2007) Numerical simulation of underwater landslide by 3D theory in time domain [in Chinese]. Proceedings of the 20th National Conference on Hydrodynamics, China Ocean Press, Beijing, pp. 721–7.
- Mayer A (1936) Characteristics of materials used in earth dam construction—stability of earth dams in cases of reservoir discharge. *Proc Second Congr Large Dams* 4:295–327
- Mehdi O, Malioche D, Chen Z, Iskander M (2015) Visualizing kinematics of dynamic penetration in granular media using transparent soils. *Geotech Test J* 5:656–672. doi:[10.1520/GTJ20140206](https://doi.org/10.1520/GTJ20140206)
- Morgenstern N (1963) Stability charts for earth slopes during rapid draw-down. *Géotechnique* 13:121–131
- Sui W, Qu H, Gao Y (2015) Modeling of grout propagation in transparent replica of rock fractures. *Geotech Test J* 5:1–9. doi:[10.1520/GTJ20140188](https://doi.org/10.1520/GTJ20140188)
- Viratjandr C, Michalowski R (2006) Limit analysis of submerged slopes subjected to water drawdown. *Can Geotech J* 43:802–814. doi:[10.1139/T06-042](https://doi.org/10.1139/T06-042)
- Wang J, Zhang H, Zhang L, Liang Y (2012) Experimental study on heterogeneous slope responses to drawdown. *Eng Geol* 147:52–56. doi:[10.1016/j.enggeo.2012.07.020](https://doi.org/10.1016/j.enggeo.2012.07.020)